Analysis of mm-Wave Detection with AlGaN/GaN HEMTs by means of Measurements and Physical and Equivalent Circuit Models

Ignacio Íñiguez-De-La-Torre, Gaudencio Paz-Martínez, Sergio García-Sánchez, Philippe Artillan, Tomás González, Javier Mateos

Analysis of mm-Wave Detection with AlGaN/GaN HEMTs by means of Measurements and Physical and Equivalent Circuit Models

I. Íñiguez-de-la-Torre*[1], G. Paz-Martínez*[2], S. García-Sánchez*[3], P. Artillan$[1], T. González*[4], J. Mateos*[5]
*Applied Physics Department, and USAL-NANOLAB, Universidad de Salamanca, 37008 Salamanca, Spain
$Univ. Grenoble Alpes, Univ. Savoie Mont Blanc, CNRS, Grenoble INP, CROMA, 38000 Grenoble, France
{[1]indy, [2]gaupaz, [3]sergio_gs, [4]tomasg, [5]javierm}@usal.es, [1]philippe.artillan@univ-smb.fr

***Abstract*—The responsivity of microwave zero-bias detectors based on GaN high electron mobility transistors (HEMTs) is measured up to 67 GHz and compared with Monte Carlo (MC) simulations. In addition, a predictive analytical closed-box model based on the measurement (or MC calculation) of the I-V curves and the S-parameters of the devices is shown to replicate the zero-bias current responsivity. The extraction of the HEMT Small-Signal Equivalent Circuit (SSEC) is also exploited to evaluate the responsivity with such closed-form expression. The comparison of the results provided by this approach with the values obtained directly from experiments and MC simulations allows not only to predict the response of the devices at frequencies above the reach of the measurements, but also to identify the physical origin of the detection and the contribution of the different SSEC elements.**

***Index Terms*—GaN high electron mobility transistors (HEMTs), Millimeter wave (mmWave) detection, Monte Carlo simulations, Small Signal Equivalent-circuit, Zero-bias detector**

I. Introduction

The excellent high-frequency and low-noise characteristics of HEMTs, as a result of the high mobility of the electrons in the 2DEG, make them the preferred choice for applications in the mm- and sub-mm-wave regime. In addition to their traditional role as amplifiers, with MMICs reaching recently 1 THz [1], Field-Effect Transistors (FETs) have recently found new applications as THz detectors, operating at frequencies well beyond their conventional cut-off frequencies [2], [3].

The initial demonstrations of THz detection by means of FETs were made using commercial GaAs HEMTs fabricated by Fujitsu [4] following the "classic" design rules for optimizing their operation as amplifiers. The theoretical background for the THz detection was based on the plasma-wave theory by Dyakonov–Shur [5], so that FETs used for THz detection have been widely labelled as "plasma-wave detectors". However, at frequencies below 1 THz, where the resistive self-mixing is at the origin of the RF detection, other approaches, such as the well-established lumped element modelling by means of a Small-Signal Equivalent Circuit (SSEC) can be better suited for its description [6]. This kind of modeling has demonstrated to correctly reproduce the results obtained in graphene FETs up to almost 1 THz [7], and it has been very helpful for the optimization of the design of the detectors. The resistive self-mixing mechanism, i.e. the rectification originated by the nonlinearity of the I_d-V_{ds} curves, is expected to be further enhanced by resonant plasma waves at THz frequencies, but only to a limited extent due to the high-frequency dependence of the channel impedance [8], not considered in the ideal plasma-wave models [9], [10]. In order account for such high-frequency mechanisms, not considered within the SSEC models, complex Monte Carlo (MC) simulations are necessary. Such studies are not frequent in the literature, only some of the authors of this paper made a qualitative exploration of the THz rectification capabilities of InGaAs HEMTs in a prior work [11].

The main objective of this contribution is to combine physical models based on MC simulations with a SSEC approach to interpret the results of RF power detection measurements in the mm-wave range, performed using a 150 nm-gate GaN HEMT [13]. In addition, a closed-box model is employed to compute the frequency dependence of the responsivity of the transistor taking as a base, on the one hand, the non-linearities of the DC curves (providing the low-frequency value of the responsivity), and, on the other, the S-parameters (providing the frequency dependence). This hybrid framework is suitable to improve modeling accuracy and efficiency, thus bridging the gap between fabrication and circuit design to allow the optimization of the performances of FET transistors when used as mm- or sub-mm-wave power detectors [14].

II. Results and Discussion

A. Device Under Test and RF Detection at Low Frequency

Our device under test is a HEMT based on an AlGaN/GaN heterojunction grown on a high-resistivity Si substrate [15] with L_g=150 nm, W=2×25 μm, fabricated with co-planar wave-guide (CPW) accesses with a 50 μm signal line and a 30 μm spacing in order to provide a 50 Ω characteristic impedance, as shown in Fig. 1. The experimental DC I-V curves of the devices under low-V_{ds} conditions, as those used in the experiments of AC power detection, are shown in Fig. 2, including the negative V_{ds} region, which plays a key role in the case of drain-injected RF power. The transfer curve reveals a threshold voltage V_{th} of around -3.8 V, which almost coincides with the bias for optimum sensitivity in RF detection. This is evidenced by the minimum of the Noise Equivalent Power

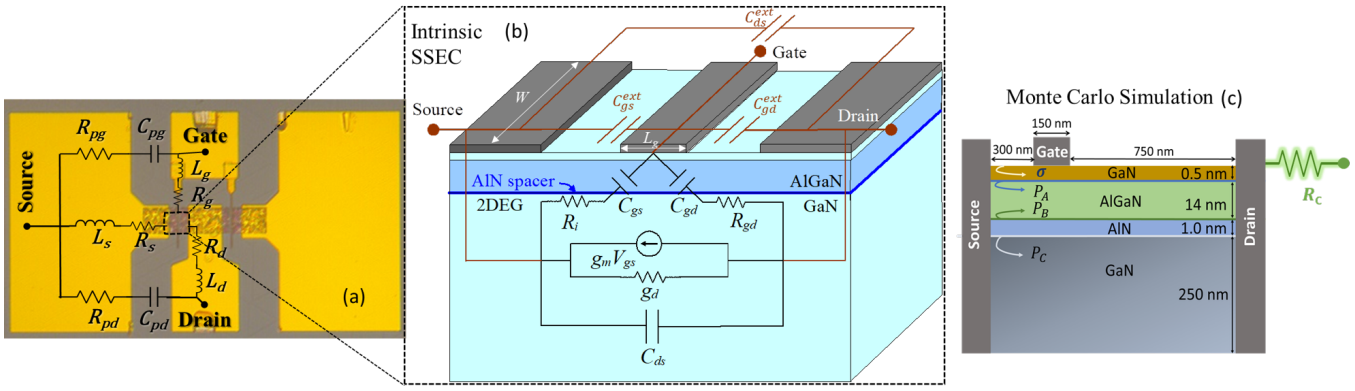

Fig. 1: (a) Coplanar wave-guide (CPW) accesses of the two-finger 250 nm-gate HEMT with the representation of the extrinsic lumped elements of its SSEC and (b) sketch of the intrinsic transistor and the corresponding intrinsic elements. In (b) it is also described the topology of the AlGaN/GaN heterostructure, consisting of a 14 nm thick $Al_{0.29}Ga_{0.71}N$ layer on a 1.73 μm thick GaN buffer, with an intercalated 1 nm AlN spacer to improve carrier confinement within the 2DEG, and a 0.5 nm thick GaN cap on the top of the heterostructure. (c) Shows the MC simulation domain, with the resistor R_c (with a value of 1.9 Ω·mm) introduced to account for the effect of the source and drain contact resistances (R_s and R_d) and that of the non-simulated source ohmic region, whose length has been reduced with respect to the real one in order to optimize the computation time. The appropriate values of the surface charges at the different interfaces (σ, P_A, P_B and P_C) have been included in the simulations to reproduce the electron sheet charge density and the square resistance of the epilayer [12].

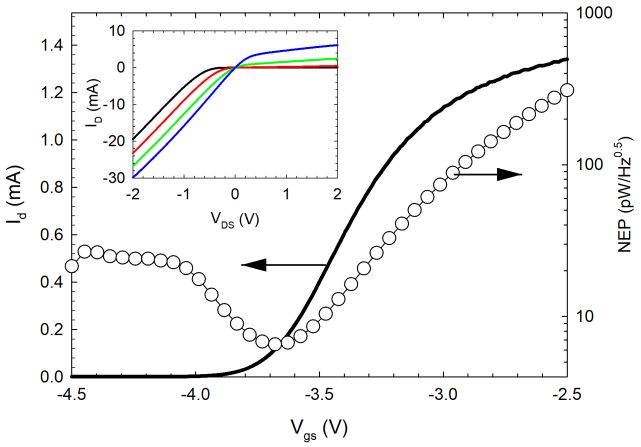

Fig. 2: Measured I_d-V_{gs} transfer characteristic for V_{ds}=0.1 V (left axis) and NEP estimated at 1 GHz (right axis). The inset shows the output curves of the transistor for V_{gs} between -4.1 V to -3.2 V in 0.3 V steps.

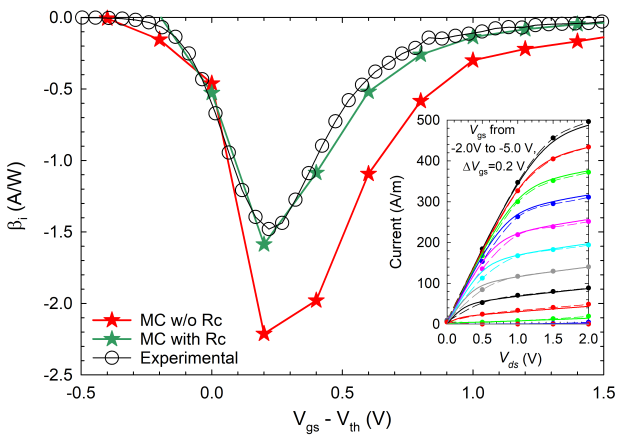

Fig. 3: Comparison of the experimental (circles) current responsivity β_i in (A/W) at low frequency as a function of V_{gs}-V_{th} with the values obtained with MC simulations (with and without the effect of R_c, green and black red stars, respectively). The experiments were performed using P_{RF}=-20 dBm at 1 GHz, while the MC simulations correspond to the response to a sinusoidal tone with amplitude of 0.25 V at 10 GHz. The inset shows the comparison of the experimental I_d-V_{ds} output characteristics (solid lines) with those obtained with MC simulations (circles, dashed lines) including contact resistances with values R_s=1.6 Ω·mm and R_d=0.3 Ω·mm.

(NEP), representing the minimum power value that a detector can sense without being hidden by its noise. As such, the NEP is defined as the rate between the detector noise and its responsivity, so that, assuming thermal noise (as expected from zero-bias detection conditions, and so using the Nyquist theorem) it can be calculated as $NEP=\frac{\sqrt{4k_BT/R}}{\beta_i}$, being R the device resistance and β_i the current responsivity. In the drain-injection configuration used in our detection experiments, β_i (in A/W) is obtained as $\beta_i(f)=\Delta I_d(f)/P_{RF}(f)$ being ΔI_d the drain current shift measured when a RF signal of P_{RF} power is injected into the drain port. Using the measured values of the responsivity, the minimum NEP provided by the studied HEMT is as low as 6.5 pW/$\sqrt{\text{Hz}}$ at V_{gs}=-3.7 V, coinciding with the maximum responsivity of around β_i=-1.5 A/W, Fig. 3.

B. Comparison with MC Simulations

In the case of MC simulations, one operates with voltages and currents and not with power waves, and the MC current responsivity β_i^{MC} is calculated as

$$\beta_i^{MC}=\frac{\Delta I_d}{P_{AC}}\left(1-|\Gamma|^2\right)=\beta_{i,opt}^{MC}\left(1-|\Gamma|^2\right), \quad (1)$$

by computing the DC average of the drain current shift, ΔI_d, in response to a single tone voltage signal applied to the drain terminal. The AC power absorbed by the transistor is computed in the time domain as the average value of the product of the instantaneous drain voltage and current $V_{ds}(t)\times I_d(t)$ provided by the MC simulation. The reflection coefficient Γ accounts for the impedance mismatch (reducing the responsivity from its optimum value $\beta_{i,opt}^{MC}$), whose low-frequency value can be calculated as $\Gamma=(R-R_0)/(R+R_0)$, being R_0=50 Ω the characteristic impedance of the transmission line.

If we compare the experimental responsivity with that obtained with MC simulations, Fig. 3, there is an important difference between the results due to the fact that MC simulations are completely intrinsic. Indeed, in order to reproduce the experimental output I_d-V_{ds} curves of the HEMT (see inset of Fig. 3), the effect of the contact resistance $R_c=R_d+R_s$=1.9 Ω·mm has to be included. This contact resistance also involves a modification of the non-linearity of the I-V curves [6], and therefore a correction has to be made to the optimum current responsivity as

$$\beta_{i,opt}^{MC+R_c}=\frac{\beta_{i,opt}^{MC}}{1+R_c g_d^{MC}}, \quad (2)$$

where g_d^{MC} is the drain conductance, obtained also with MC simulations. Moreover, R_c has to be taken into account in the calculation of the reflection coefficient. The result of eq. (2) perfectly reproduces the dependence on V_{gs} of the experimental low-frequency values of β_i, Fig. 3. Note that we have shifted the x-axis according to the values of V_{th} in order to allow the comparison with the intrinsic MC simulations.

C. Closed-Form Expression for High-Frequency Responsivity

In [16] we proposed a generic high-frequency model of two-port RF detectors in which we derive a closed-form expression (CFE) based on (i) the static conductance coefficients, defined as $g_{ij}=\partial^{(i+j)}I_d/\partial^i V_{gs}\partial^j V_{ds}$, extracted from the I_d-V_{ds} curves, and (ii) the frequency-dependent S-parameters, able to replicate the device responsivity, particularized in the following equation for the case of drain injection:

$$\beta_i=\frac{R_0}{2}\left(g_{20}|S_{12}|^2+g_{02}|1+S_{22}|^2+2g_{11}\Re[S_{12}^*(1+S_{22})]\right). \quad (3)$$

Since g_{20} is null for V_{ds}=0, as in the zero-bias conditions used here, only the last two terms are significant, one (proportional to g_{02}) corresponding to the direct drain voltage swing and the other (proportional to g_{11}) associated to the gate voltage swing, which appears due to the drain-gate coupling. The results of the CFE formalism, Fig. 4 (solid black line), accurately reproduce the frequency dependence of the experiments.

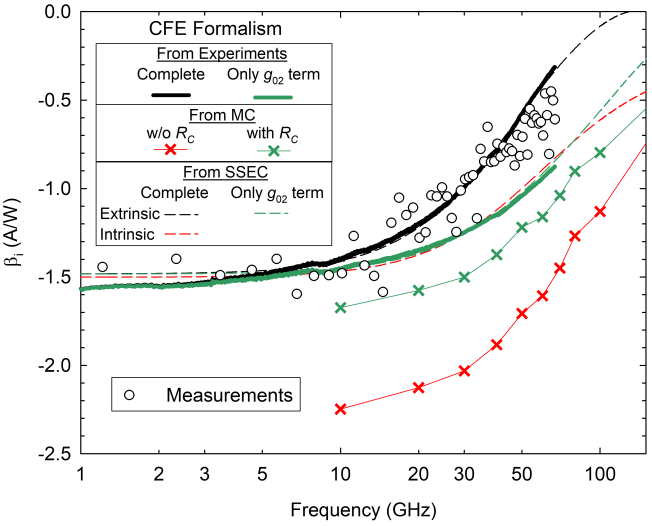

Fig. 4: Comparison of the experimental results of β_i vs. frequency with the results of the CFE formalism given by eq. (3) taking the values of the I-V curves and S-parameters from different sources: measurements (black solid line), intrinsic and extrinsic SSEC (dashed lines) and MC simulations with and without including the effect of R_C (green and red crosses, respectively). The results obtained with the extrinsic SSEC for the g_{02} term of the CFE are also shown for comparison (green dashed line). The gate bias is V_{gs}-V_{th}=0.2 V.

D. Comparison with MC Simulations

In the case on MC simulations, the S_{ij} parameters are computed from the complex Y-matrix. The Y_{ij} parameters are directly extracted from the current response when applying a single-tone voltage signal with varying frequency to the drain and gate terminals. The comparison between the measured frequency dependence of β_i and that obtained with MC simulations for the V_{gs} value where the maximum responsivity is achieved (V_{gs}=-3.65 V), Fig. 4, displays a significant overestimation of the simulated responsivity in all the frequency span. Apart from the non-inclusion of the contact resistance, R_C, which explains the discrepancy at low frequency, the effect of the extrinsic capacitances shown in Figs. 1(a) and (b), not included in the MC simulation domain, leads also to a higher cutoff frequency in the simulations. This is better observed when including the effect of R_C on the g_{ij} coefficients and the S_{ij} parameters, both involved in the computation of β_i by means of the CFE of eq. (3), see green crosses on Fig. 4, which are able to reasonably well reproduce the measured low frequency value of the responsivity, but with a higher cutoff frequency.

If one just includes the term on g_{02} on the CFE calculation (solid green thick line), the result that better agrees with that of the MC results containing the effect of R_c (green crosses). Indeed, the term on g_{11} associated to the capacitive coupling

between gate and drain, intensifies the high-frequency roll off of β_i, since it has positive sign and partially compensates the negative value of the term on g_{02}, thus contributing to decrease the cut-off frequency of the detection [16]. This improved configuration obtained by suppressing the g_{11} term on the CFE can be practically implemented by connecting a large capacitor between gate and source terminals, acting as a short circuit for the RF component at the gate, thus avoiding any possible V_{gs} swing and cancelling the gate-drain coupling.

E. Small-Signal Equivalent Circuit Analysis

For a simpler modeling of the detection we have also calculated the value of β_i using the SSEC model shown in Figs. 1(a) and (b) to obtain the values of the S-parameters of the GaN HEMT under study, to be inserted into the CFE of eq. (3). The values of the lumped elements of the SSEC (see Table I) have been determined using the well-known Dambrine's cold-FET method [17] and with the help of the physical insight provided by the results of MC simulations.

TABLE I: Values of the elements of the SSEC for V_{gs}=-3.65 V.

Intrinsic elements	Value
C_{gd} (fF/mm)	233.8
C_{gs} (fF/mm)	301
C_{ds} (fF/mm)	0.06
R_{gd} ($\Omega\times$mm)	3.5
R_i ($\Omega\times$mm)	6.43
g_d (mS/mm)	1.84

Extrinsic elements	Value
R_g=R_d=R_s (Ω)	1.0
L_g (pH)	20.0
L_d (pH)	25.0
L_s (pH)	10.0
C_{pg} (fF)	8.0
C_{pd} (fF)	11.0
C_{gd}^{ext} (fF)	6.0
C_{gs}^{ext} (fF)	8.45
C_{ds}^{ext} (fF)	4.0

Fig. 4 confirms the good agreement obtained when comparing the experimental values of β_i and those provided by the complete SSEC model, and also in the case of the values corresponding to the g_{02} term of the CFE. On the other hand, taking just the intrinsic section of the SSEC, Fig. 1(b) [without the parasitic elements of the CPW accesses of Fig. 1(a) and without the three capacitances denoted as C^{ext} in Fig. 1(b)], we find the surprising result that the values of β_i are quite similar to those associated to the direct drain detection (the term proportional to g_{02} in the CFE). That means that the gate-drain coupling happens mainly through the extrinsic capacitance C_{gd}^{ext}.

III. Conclusions

Thanks to the combination of experimental measurements, physics based MC simulations, SSEC models and an analytical CFE formalism we provide insight into the FET-based RF power detection mechanisms. In this contribution we focus on the effect of the contact resistances, which decrease the low-frequency value of the responsivity β_i, and the parasitic capacitances, which decrease the cutoff frequency of the detection. Also, the comparison between MC simulations and measurements demonstrates that the gate-drain coupling mechanism happens mainly through the extrinsic capacitance C_{gd}^{ext}. This leads to the decrease of the overall responsivity in drain-injection conditions at high frequency.

Acknowledgment

This work has been partially supported through grant PID2020-115842RB-I00 funded by MCIN/AEI/10.13039/501100011033 and the Junta de Castilla y León and FEDER through project SA136P23. This research has made use of the high performance computing resources of the Castilla y León Supercomputing Center (SCAYLE, www.scayle.es), financed by the European Regional Development Fund (ERDF).

References

[1] X. Mei, W. Yoshida, M. Lange, *et al.*, "First demonstration of amplification at 1 THz using 25-nm InP high electron mobility transistor process," *IEEE Electron Dev. Lett.*, vol. 36, no. 4, pp. 327–329, 2015.

[2] F. Aniel, G. Auton, D. Cumming, *et al.*, *Terahertz electronic devices*. Springer International Publishing, 2023.

[3] E. Javadi, D. B. But, K. Ikamas, J. Zdanevičius, W. Knap, and A. Lisauskas, *Sensors*, vol. 21, no. 9, 2021.

[4] R. Weikle, J.-Q. Lü, M. Shur, and M. Dyakonov, "Detection of microwave radiation by electronic fluid in high electron mobility transistors," *Electronics Letters*, vol. 32, 2148–2149(1), 23 1996.

[5] M. Dyakonov and M. Shur, "Plasma wave electronics: Novel terahertz devices using two dimensional electron fluid," *IEEE Transactions on Electron Devices*, vol. 43, no. 10, pp. 1640–1645, 1996.

[6] M. A. Andersson and J. Stake, "An accurate empirical model based on volterra series for fet power detectors," *IEEE Trans. Microw. Theory Techn.*, vol. 64, no. 5, pp. 1431–1441, 2016.

[7] X. Yang, A. Vorobiev, K. Jeppson, and J. Stake, "Describing broadband terahertz response of graphene FET detectors by a classical model," *IEEE Trans. THz Sci. Technol.*, vol. 10, no. 2, pp. 158–166, 2020.

[8] M. Bauer, A. Rämer, S. A. Chevtchenko, *et al.*, "A high-sensitivity algan/gan hemt terahertz detector with integrated broadband bow-tie antenna," *IEEE Trans. THz Sci. Technol.*, vol. 9, pp. 430–444, 2019.

[9] W. Knap, F. Teppe, Y. Meziani, *et al.*, "Plasma wave detection of sub-terahertz and terahertz radiation by silicon field-effect transistors," *Applied Physics Letters*, vol. 85, no. 4, pp. 675–677, Jul. 2004.

[10] J. M. Caridad, O. Castelló, S. M. López Baptista, *et al.*, "Room-temperature plasmon-assisted resonant THz detection in single-layer graphene transistors," *Nano Letters*, vol. 24, no. 3, pp. 935–942, 2024.

[11] J. Mateos and T. Gonzalez, "Plasma enhanced terahertz rectification and noise in ingaas hemts," *IEEE Trans. THz Sci. Technol.*, vol. 2, no. 5, pp. 562–569, 2012.

[12] H. Sánchez-Martín, I. Íñiguez-de-la Torre, S. García-Sánchez, J. Mateos, and T. González, "Monte Carlo analysis of thermal effects in the DC and AC performance of AlGaN/GaN HEMTs," *Solid-State Electronics*, vol. 193, p. 108 289, 2022, ISSN: 0038-1101.

[13] G. Paz-Martínez, I. Íñiguez-de-la Torre, H. Sánchez-Martín, T. González, and J. Mateos, "Analysis of GaN-Based HEMTs operating as RF detectors over a wide temperature range," *IEEE Trans. Microw. Theory Techn.*, vol. 71, no. 7, pp. 3126–3135, 2023.

[14] G. Wang, H. Gu, X. Li, *et al.*, "Terahertz sensing and communication towards future intelligence connected networks," 2022.

[15] P. Altuntas, F. Lecourt, A. Cutivet, *et al.*, "Power performance at 40 GHz of AlGaN/GaN high-electron mobility transistors grown by molecular beam epitaxy on Si (111) substrate," *IEEE Electron Device Lett.*, vol. 36, no. 4, pp. 303–305, 2015.

[16] G. Paz-Martínez, P. Artillan, J. Mateos, E. Rochefeuille, T. González, and I. Íñiguez-de-la Torre, "A closed-form expression for the frequency dependent microwave responsivity of transistors based on the I-V curve and S-Parameters," *IEEE Trans. Microw. Theory Techn.*, vol. 72, no. 1, pp. 415–420, 2024.

[17] G. Dambrine, A. Cappy, F. Heliodore, and E. Playez, "A new method for determining the FET small-signal equivalent circuit," *IEEE Trans. Microw. Theory Techn.*, vol. 36, no. 7, pp. 1151–1159, 1988.